Apoptosis (2019) 24:862–877
https://doi.org/10.1007/s10495-019-01565-5

Defining the role of cytoskeletal components in the formation of apoptopodia and apoptotic bodies during apoptosis

Sarah Caruso[1] · Georgia K. Atkin-Smith[1] · Amy A. Baxter[1] · Rochelle Tixeira[1] · Lanzhou Jiang[1] · Dilara C. Ozkocak[1] · Jascinta P. Santavanond[1] · Mark D. Hulett[1] · Peter Lock[1] · Thanh Kha Phan[1] · Ivan K. H. Poon[1]

Published online: 5 September 2019

Abstract

During apoptosis, dying cells undergo dynamic morphological changes that ultimately lead to their disassembly into fragments called apoptotic bodies (ApoBDs). Reorganisation of the cytoskeletal structures is key in driving various apoptotic morphologies, including the loss of cell adhesion and membrane bleb formation. However, whether cytoskeletal components are also involved in morphological changes that occur later during apoptosis, such as the recently described generation of thin apoptotic membrane protrusions called apoptopodia and subsequent ApoBD formation, is not well defined. Through monitoring the progression of apoptosis by confocal microscopy, specifically focusing on the apoptopodia formation step, we characterised the presence of F-actin and microtubules in a subset of apoptopodia generated by T cells and monocytes. Interestingly, targeting actin polymerisation and microtubule assembly pharmacologically had no major effect on apoptopodia formation. These data demonstrate apoptopodia as a novel type of membrane protrusion that could be formed in the absence of actin polymerisation and microtubule assembly.

Keywords Apoptotic bodies · Apoptotic cell disassembly · Apoptotic morphology · Apoptopodia · Cytoskeletal components · Membrane protrusions

Introduction

Cellular membrane protrusions involving dynamic extensions of the plasma membrane vary greatly in morphology, regulation and function. Well-characterised membrane protrusions generated by both resting and activated cells include filopodia [1], lamellipodia [2], membrane nanotubes [3] and invadopodia [4]. Such protrusions are generally actin-rich and their formation is dependent on polymerisation of actin monomers leading to the assembly of filamentous actin (F-actin) [5–9]. Notably, F-actin disassembly and reassembly is especially important for membrane protrusions such as lamellipodia and filopodia that facilitate cell motility [8, 10, 11], where F-actin assembly has been shown to predominantly occur at the leading edge of the extending protrusion [11, 12]. F-actin is also a key component of membrane nanotubes, which are generated from F-actin initiating protrusions [7, 9, 13]. In the case of lamellipodia, actin branching in addition to actin polymerisation plays an important role in the formation of a dynamic protrusive actin network [11, 14, 15]. Directed actin polymerisation combined with actin depolymerisation at opposing ends of actin filaments, a process known as treadmilling, has been shown to be a key process underpinning extension of the leading edge of lamellipodia [16–18]. While most membrane protrusions rely less on microtubules to drive their formation, particularly in the case of lamellipodia and filopodia [5, 19–21], tubulin-based microtubules have been implicated in exerting the forces required for endothelial cell invadopodia to protrude and extend into a 3D collagen matrix [22].

In addition to membrane protrusions generated by healthy viable cells, new types of protrusions have recently been

Sarah Caruso and Georgia K. Atkin-Smith have contributed equally to this work.

Electronic supplementary material The online version of this article (https://doi.org/10.1007/s10495-019-01565-5) contains supplementary material, which is available to authorized users.

✉ Ivan K. H. Poon
i.poon@latrobe.edu.au

[1] Department of Biochemistry and Genetics, La Trobe Institute for Molecular Science, La Trobe University, Melbourne, VIC 3086, Australia

described that form exclusively during the progression of apoptosis (a form of programmed cell death) when the apoptotic cell undergoes disassembly [23–26]. After the induction of apoptosis, apoptotic cells can undergo a series of morphological changes including plasma membrane blebbing (step 1 of apoptotic cell disassembly), apoptotic membrane protrusion formation (step 2) and generation of membrane-bound extracellular vesicles known as apoptotic bodies (ApoBDs) (step 3) [24, 26–28]. Apoptotic membrane protrusions can exhibit a diverse range of morphologies including thin string-like structures such as those generated by apoptotic T cells (called apoptopodia), or a 'beads-on-a-string' like structures such as those formed by apoptotic monocytes (beaded-apoptopodia) [24, 26]. Apoptopodia often associate with ApoBDs and can undergo fragmentation to release an abundance of ApoBDs during the final stages of the apoptotic cell disassembly process [24, 26]. Although the membrane channel pannexin 1 (PANX1) was recently described as a negative regulator of apoptopodia formation [24, 26], molecular components involved in driving the formation of these protrusions are yet to be fully defined.

Given the importance of the dynamic cytoskeletal behaviour in the formation of a variety of cellular protrusions and in other morphological stages of apoptosis (e.g. during membrane blebbing) [29–31], we investigated the potential contribution of actin and tubulin cytoskeletal components in the formation of apoptotic membrane protrusions. We used confocal live imaging approaches to characterise the apoptotic membrane protrusions produced by apoptotic T cells, monocytes and epithelial cells, and assessed the requirement of actin polymerisation and microtubule assembly in protrusion formation during apoptotic cell disassembly. These studies clearly identified a subset of apoptopodia generated by Jurkat T cells and THP-1 monocytic cells which contained F-actin and microtubules. Surprisingly however, actin polymerisation was found to be not essential for the formation of apoptopodia, while microtubule assembly may play a minor role in this process. Notably, pharmacological inhibition of microtubule assembly also had minimal effects on ApoBD formation in all cell types tested. Furthermore, we showed that vimentin, a component of the intermediate filament cytoskeleton, is unlikely to play a major role in the formation of apoptopodia and ApoBDs by apoptotic Jurkat T cells. Together, these findings highlight apoptopodia as a unique subclass of membrane protrusion whereby their formation is independent of key cytoskeletal comments such as F-actin.

Results

T cells and monocytes form apoptotic membrane protrusions in cell suspension and in 3D cultures

The apoptotic cell disassembly process in T cells and monocytes has been described in detail [24, 26] and involves three morphologically distinct steps (Fig. 1a). As mentioned above, step 1 of the disassembly process includes the formation of circular bulges on the plasma membrane called blebs as a result of actomyosin contraction, and is regulated by Rho-associated coiled coil containing kinase 1 (ROCK1) [29, 30, 32]. This is followed by step 2 of apoptotic cell disassembly with the formation of apoptopodia/beaded-apoptopodia (Fig. 1a). Previously, the formation of apoptopodia and beaded-apoptopodia by apoptotic T cells and monocytes, respectively, were largely described in cells suspended in culture media [23, 26, 28]. However, whether apoptopodia possess the physical characteristics to form in 3D matrices that mimic the physiological environment of tissue, similar to other types of cellular protrusions like invadopodia [22] has remained unclear. Therefore, we initially monitored the formation of apoptopodia by human Jurkat T cells in a 3D culture model (cells were cultured in the matrix medium Cultrex®, consisting largely of the extracellular matrix proteins laminin and Collagen IV) during the progression of apoptosis by live differential interference contrast (DIC) microscopy. Jurkat T cells were induced to undergo apoptosis by UV irradiation and treated with trovafloxacin (trova, a PANX1 inhibitor) to promote apoptopodia-mediated apoptotic cell disassembly [26]. Similar to cells undergoing apoptosis in suspension, apoptotic Jurkat T cells also clearly generated apoptopodia in Cultrex® (Fig. 1b). Importantly, similar results were also observed for primary cultures of mouse thymocytes undergoing UV-induced apoptosis (Fig. 1c). Next, we monitored the disassembly of human apoptotic THP-1 monocytic cells and demonstrated that THP-1 cells were able to generate characteristic beaded-apoptopodia in suspension and in 3D cultures, ~ 3 h post UV irradiation (Fig. 1d). Furthermore, apoptotic primary mouse monocytes were also able to generate beaded-apoptopodia in 3D cultures, ~ 3 h post UV irradiation (Fig. 1e). Together, these data indicate that the formation of apoptotic membrane protrusions is not limited to cells in suspension but also extends to those grown in 3D environments. Notably, for the remainder of this study, the cell suspension model was employed to monitor the role of cytoskeletal components in the formation of protrusions and ApoBDs.

We next measured the rate at which Jurkat T cell and THP-1 monocyte apoptopodia extend. Using live time-lapse DIC microscopy, the longest protrusion generated

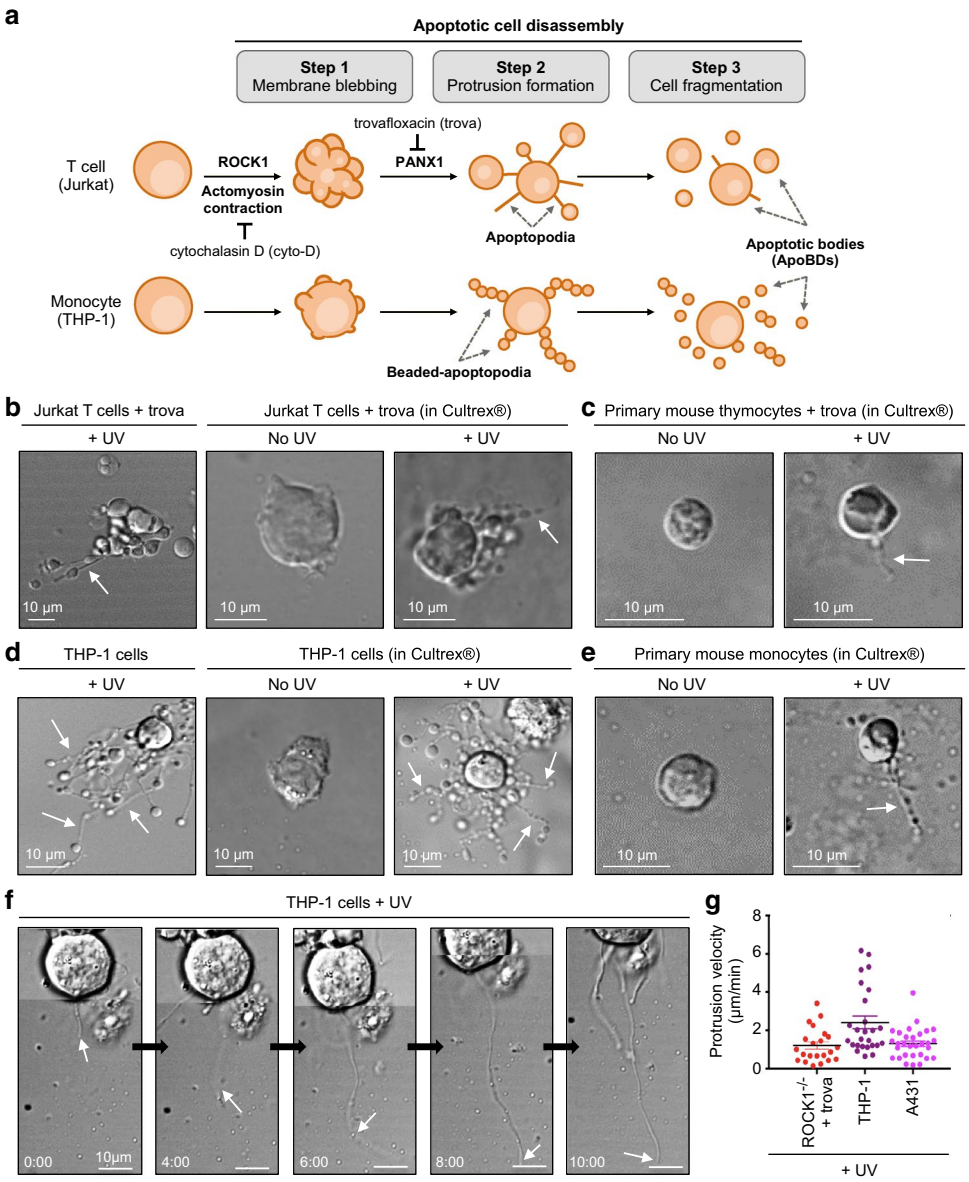

Fig. 1 Characterisation of T cell and monocyte apoptopodia in suspension and in 3D culture. **a** Schematic diagram detailing the three steps of apoptotic cell disassembly for T cells and monocytes including apoptotic membrane blebbing, apoptopodia formation and ApoBD release. **b** Representative DIC microscopy images of viable and apoptotic Jurkat T cells in Cultrex® 3D matrix, and apoptotic Jurkat T cells in suspension. Jurkat T cells were induced to undergo apoptosis by UV irradiation for ~4 h and in the presence of 40 µM trovafloxacin (trova), a PANX1 inhibitor to promote apoptopodia-mediated disassembly. **c** Representative DIC microscopy images of viable and apoptotic primary mouse thymocytes in Cultrex® 3D matrix, ~4 h post UV irradiation, 40 µM trova. **d** Representative DIC microscopy images of viable and apoptotic THP-1 monocytes in Cultrex® 3D matrix, and apoptotic THP-1 cells in suspension ~ 3 h post UV irradiation. **e** Representative DIC microscopy images of viable and apoptotic primary mouse $CD14^+$ monocytes in Cultrex® 3D matrix, ~ 3 h post UV irradiation. **f** Time-lapse DIC microscopy monitoring apoptotic (UV-irradiated) THP-1 monocyte protrusion velocity. **g** Average protrusion velocity rate of apoptotic (UV-irradiated) $ROCK1^{-/-}$ Jurkat T cells treated with 40 µM trova (n = 22 cells), THP-1 monocytic cells (n = 30) and A431 epithelial cells (n = 26). Error bars represent SEM. **b**–**e** Data are representative of at least two independent experiments. Apoptosis induced by 150 mJ/cm^2 UV irradiation.

by individual apoptotic cells was monitored from the initiation of protrusion formation to the maximal protrusion extension prior to any fragmentation or retraction events (Fig. 1f). To monitor apoptopodia formation in Jurkat T cells in this study, we developed a model by using $ROCK1^{-/-}$ Jurkat T cells which bypass the membrane blebbing stage of apoptotic cell disassembly (ROCK1 is the key regulator of membrane blebbing for Jurkat T cells) [33], allowing clear identification of apoptopodia formation when cells were induced to undergo apoptosis and in

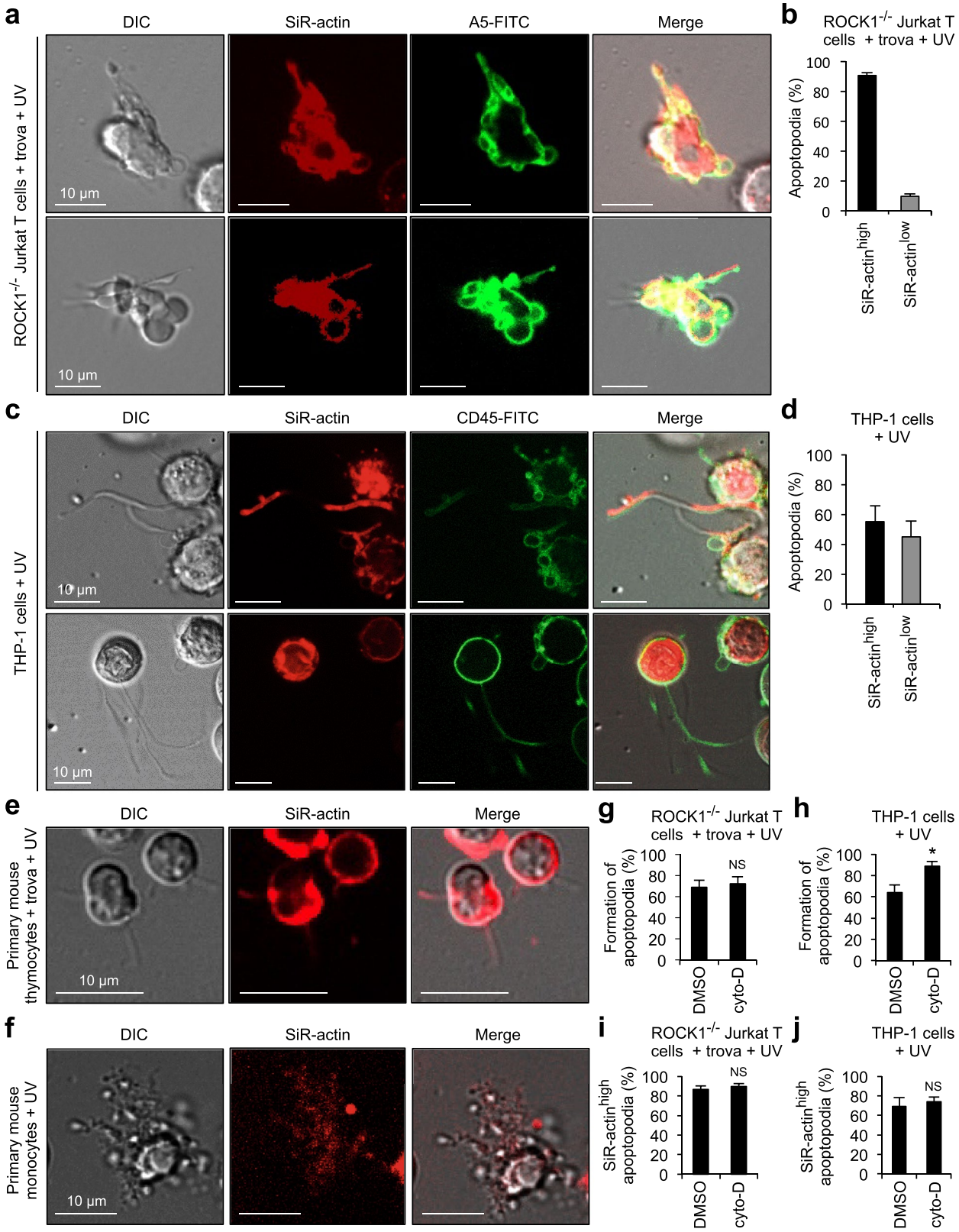
a
DIC
SiR-actin
A5-FITC
Merge
ROCK1-/- Jurkat T cells + trova + UV
10 μm
b
ROCK1-/- Jurkat T cells + trova + UV
Apoptopodia (%)
SiR-actinhigh
SiR-actinlow
c
DIC
SiR-actin
CD45-FITC
Merge
THP-1 cells + UV
d
THP-1 cells + UV
e
Primary mouse thymocytes + trova + UV
f
Primary mouse monocytes + UV
g
Formation of apoptopodia (%)
NS
DMSO
cyto-D
h
*
i
SiR-actinhigh apoptopodia (%)
j

◂**Fig. 2** The role of actin polymerisation in apoptotic membrane protrusion formation. **a** Representative confocal microscopy images of apoptotic ROCK1$^{-/-}$ Jurkat T cells (40 µM trova) stained with the fluorescent probe SiR-actin (red, F-actin) and A5-FITC (green, Ptd-Ser exposure, indicative of the plasma membrane). **b** Percentage of apoptotic ROCK1$^{-/-}$ Jurkat T cells with protrusions containing SiR-actin staining (i.e. SiR-actin^{high}). **c** Representative confocal microscopy images of apoptotic THP-1 monocytes stained with SiR-actin (red) and CD45-FITC (green, indicative of the plasma membrane). **d** Percentage of apoptotic THP-1 monocytes with protrusions containing SiR-actin staining. Confocal microscopy images of apoptotic primary mouse thymocytes (40 µM trova) **e** or, apoptotic primary mouse CD14^{+} monocytes **f** stained with SiR-actin. **g** Percentage of apoptotic ROCK1$^{-/-}$ Jurkat T cells (40 µM trova) forming membrane protrusions, with and without 10 µM cytochalasin D (cyto-D) treatment. **h** Percentage of apoptotic THP-1 cells forming membrane protrusions with and without 10 µM cyto-D treatment. **i** Percentage of apoptotic ROCK1$^{-/-}$ Jurkat T cells (40 µM trova) that generate protrusions containing SiR-actin staining in the presence or absence of 10 µM cyto-D treatment. **j** Percentage of apoptotic THP-1 cells that generate protrusions containing SiR-actin staining in the presence or absence of 10 µM cyto-D treatment. Error bars represent SEM (n = 3), data are representative of three independent experiments, NS = $p \geq 0.05$, $^{*}p < 0.05$, unpaired Student's two-tailed *t* test. Apoptosis induced by 150 mJ/cm^2 UV irradiation.

the presence of trova to promote apoptopodia formation. It should be noted that THP-1 monocytes can generate an abundance of apoptopodia under basal conditions [24]. The average velocity of protrusion extension was 1.21 µm/min (SEM ± 0.19) and 2.42 µm/min (SEM ± 0.33) for Jurkat T cells and THP-1 monocytes, respectively (Fig. 1g). Notably, the velocity of apoptopodia extension recorded is comparable to the velocity of growing microtubules [34], but considerably higher than the velocity of F-actin polymerisation [35].

The role of F-actin in apoptotic membrane protrusion formation

To determine whether F-actin, a key cytoskeletal component, may be involved in the formation of apoptopodia by Jurkat T cells or THP-1 monocytes, we utilised the cell permeable probe SiR-actin to monitor F-actin localisation and a plasma membrane staining approach (using either annexin A5 (A5) or anti-CD45) to help visualise apoptopodia. First, we monitored apoptotic Jurkat T cells at ~ 4 h post UV-induced apoptosis (using the same cell model as described above whereby Jurkat T cells are deficient in ROCK1 and treated with the PANX1 inhibitor trova) and found that both F-actin rich (SiR-actin^{high}) and F-actin depleted (SiR-actin^{low}) protrusions could be observed, with approximately 90% of apoptopodia-forming cells capable of producing F-actin rich apoptopodia (Fig. 2a, b, Supplementary video 1). Using a similar experimental approach, we observed apoptotic THP-1 monocytes at ~ 3 h post UV-induced apoptosis and approximately 55% of these apoptopodia-forming cells produced protrusions containing F-actin (Fig. 2c, d). It should be noted that quantification was performed on z-stack images to ensure the entire apoptopodia was captured (Supplementary video 1 and 2). These results were consistent with primary cells undergoing apoptosis whereby apoptotic primary mouse thymocytes and bone marrow-derived monocytes were also able to generate apoptopodia containing F-actin (Fig. 2e, f). To investigate whether actin polymerisation contributed to the formation of apoptopodia, Jurkat T cells were treated with cytochalasin D (cyto-D) to inhibit actin polymerisation during the progression of apoptosis and monitored by live DIC microscopy. Interestingly, at 4 h post apoptosis induction, cyto-D treatment had no effect on the percentage of apoptotic cells forming apoptopodia (Fig. 2g, Supplementary Fig. 1). Furthermore, THP-1 monocytes treated with cyto-D during the progression of apoptosis resulted in an increase in the percentage of apoptopodia-forming cells (Fig. 2h, Supplementary Fig. 2). To ensure the effect we observed was not due to microtubule assembly compensating for the loss of actin polymerisation, we also quantified apoptopodia formation when both actin polymerisation and microtubule assembly were blocked simultaneously by cyto-D and noco treatment, respectively, and we found no decrease in the percentage of apoptotic cells forming protrusions (Supplementary Fig. 3a, b). Notably, treatment of Jurkat T and THP-1 cells with cyto-D during apoptosis also did not alter the percentage of apoptopodia that contained F-actin (Fig. 2i, j). Taken together, these results highlight that although apoptopodia may contain F-actin, actin polymerisation is not necessary for the formation of such apoptotic membrane protrusions.

The role of microtubules in apoptotic membrane protrusion formation

As our data suggests that actin polymerisation may not play a key role in driving apoptopodia formation, we next examined the role of another key component of the cytoskeleton, microtubules, in the formation of apoptopodia. Using the same cell models as described above, we stained Jurkat T cells and THP-1 monocytes with the cell permeable probe SiR-tubulin to monitor the distribution of microtubules during the apoptotic cell disassembly process. Apoptotic Jurkat T cells generated both microtubule rich (SiR-tubulin^{high}) and microtubule depleted (SiR-tubulin^{low}) apoptopodia, whereby approximately 61% of apoptopodia-forming cells produced microtubule rich apoptopodia (Fig. 3a, b, Supplementary video 3). When monitoring apoptotic THP-1 monocytes, only ~ 20% of all apoptopodia-forming apoptotic cells could generate microtubule rich apoptopodia (Fig. 3c, d, Supplementary video 4). It should be noted that apoptotic primary mouse thymocytes and monocytes also generated apoptopodia containing microtubules (Fig. 3e, f). We next

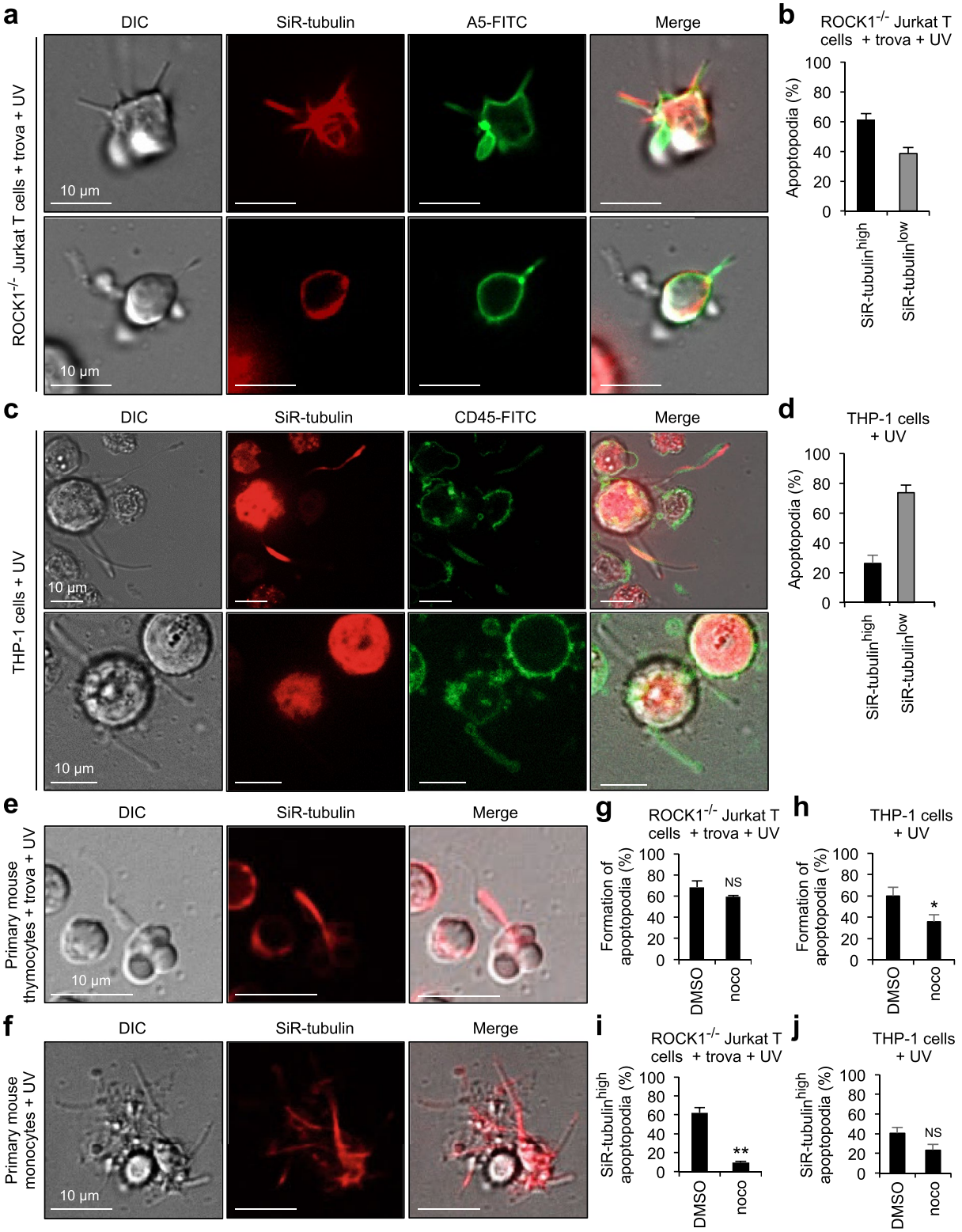

treated Jurkat T cells with nocodazole (noco), a microtubule destabilising drug, immediately after the induction of apoptosis and monitored cell disassembly by time-lapse DIC microscopy. Noco treatment had no effect on the percentage of apoptotic Jurkat T cells forming apoptopodia (Fig. 3g). In contrast, noco treatment partially impaired apoptopodia

◂**Fig. 3** The role of microtubule assembly in apoptotic membrane protrusion formation. **a** Representative confocal microscopy images of apoptotic ROCK1$^{-/-}$ Jurkat T cells (40 µM trova) stained with the fluorescent probe SiR-tubulin (red, microtubules) and A5-FITC (green, PtdSer exposure, plasma membrane). **b** Quantification of apoptotic ROCK1$^{-/-}$ Jurkat T cells with protrusions containing SiR-tubulin staining (i.e. SiR-tubulin^{high}). **c** Representative confocal microscopy images of apoptotic THP-1 monocytes stained with SiR-tubulin (red) and CD45-FITC (green, plasma membrane). **d** Quantification of apoptotic THP-1 cells with protrusions containing SiR-tubulin staining. Confocal microscopy images of apoptotic primary mouse thymocytes (40 µM trova) **e** or apoptotic primary mouse monocytes **f** stained with SiR-tubulin (red). **g** Percentage of apoptotic ROCK1$^{-/-}$ Jurkat T cells (40 µM trova) forming membrane protrusions in the presence or absence of 20 µg/mL nocodazole (noco). **h** Percentage of apoptotic THP-1 cells that generate membrane protrusions in the presence or absence of 20 µg/mL noco. **i** Percentage of apoptotic ROCK1$^{-/-}$ Jurkat T cells (40 µM trova) with protrusions containing SiR-tubulin staining in the presence or absence of 20 µg/mL noco. **i** Percentage of apoptotic THP-1 monocytes with protrusions containing SiR-tubulin staining in the presence or absence of 20 µg/mL noco treatment. Error bars represent SEM (n = 3), data are representative of three independent experiments, NS = $p \geq 0.05$, *$p < 0.05$, **$p < 0.01$, unpaired Student's two-tailed t test. Apoptosis was induced by 150 mJ/cm^2 UV irradiation.

formation by apoptotic THP-1 monocytes (Fig. 3h). It should be noted that noco treatment was effective in reducing the percentage of microtubule rich apoptopodia generated by Jurkat T cells and to a lesser extent for THP-1 monocytes (Fig. 3i, j), validating that noco was able to destabilise microtubules in our experimental setting. Furthermore, activity of noco on Jurkat T cells was also confirmed by cell cycle arrest analysis (Supplementary Fig. 4). Collectively, these data demonstrate that microtubules are present in a subset of apoptopodia generated by apoptotic T cells and monocytes, and microtubules may partially contribute to the formation of apoptopodia by apoptotic THP-1 monocytes but not Jurkat T cells.

Disruption of actin polymerisation but not microtubule assembly inhibits ApoBD formation

To further examine the role of cytoskeletal components in the overall apoptotic cell disassembly process, we monitored the formation of ApoBDs by T cells and monocytes in the presence of inhibitors of actin and tubulin polymerisation. Blocking actin polymerisation by treatment with either cyto-D or lantrunculin A inhibited ApoBD formation by apoptotic Jurkat T cells and THP-1 monocytes (Fig. 4a–d). Rather than reducing ApoBD formation through targeting apoptotic membrane protrusion formation, this effect is likely attributed to blocking membrane blebbing (i.e. step 1 of apoptotic cell disassembly) as this process is dependent on actomyosin contraction [29]. Therefore, while actin polymerisation may not be essential for apoptopodia formation (Fig. 2g, h), it is necessary for the apoptotic cell disassembly process. In contrast, inhibition of microtubule assembly by noco or demecolcine (a drug that depolymerises microtubules; activity validated by cell cycle arrest analysis as shown in Supplementary Fig. 4) had no major impact on the formation of ApoBDs by both apoptotic Jurkat T cells and THP-1 monocytes (Fig. 4e, h), suggesting that the assembly of microtubules is not necessary for apoptotic cell disassembly.

Reduction in vimentin expression does not affect the formation of apoptotic membrane protrusions and ApoBDs by Jurkat T cells

Intermediate filament components such as vimentin have been shown to play a role in the formation of cellular protrusions including invadopodia and lamellipodia, and have important interactions with actin and tubulin in these settings [6, 36, 37]. Therefore, to investigate the role of vimentin in apoptotic membrane protrusion formation, vimentin was targeted using a doxycycline (dox)-inducible CRISPR/Cas9-based approach in Jurkat T cells (isgVimentin cells). Dox treatment of isgVimentin cells resulted in a decrease in vimentin expression compared to untreated isgVimentin control cells, as detected by immunoblotting (Fig. 5a). When monitoring apoptotic cell disassembly by flow cytometry, reduction in vimentin expression did not alter ApoBD formation by Jurkat T cells, in either the absence or presence of the PANX1 inhibitor trova (Fig. 5b). Furthermore, Jurkat T cells generated an abundance of apoptopodia, ~4 h post UV irradiation, despite dox treatment and thus reduction in vimentin expression, as monitored by live DIC microscopy (Fig. 5c). Taken together, these data suggest that vimentin is unlikely to play a key role in the disassembly of apoptotic Jurkat T cells.

The role of actin and tubulin in apoptotic A431 cell disassembly

In addition to apoptopodia and beaded-apoptopodia, Moss et al. previously described a rigid class of apoptotic membrane protrusions termed microtubule spikes [25]. As the name suggests, microtubule spikes are highly enriched with microtubules and have only been observed on a few cell types, in particular the epithelial carcinoma cell line, A431 [25]. Therefore, we sought to investigate the cytoskeletal components of the so-called microtubule spikes to allow comparison with apoptopodia as described above. First, we examined UV-irradiated A431 cells by time-lapse DIC microscopy and found that apoptotic cells were able to generate rigid apoptotic membrane protrusions as previously described (Fig. 6a). Notably, the protrusion velocity of A431 cell apoptotic membrane protrusions were also determined revealing an average velocity of 1.30 µm/min (SEM ± 0.15)

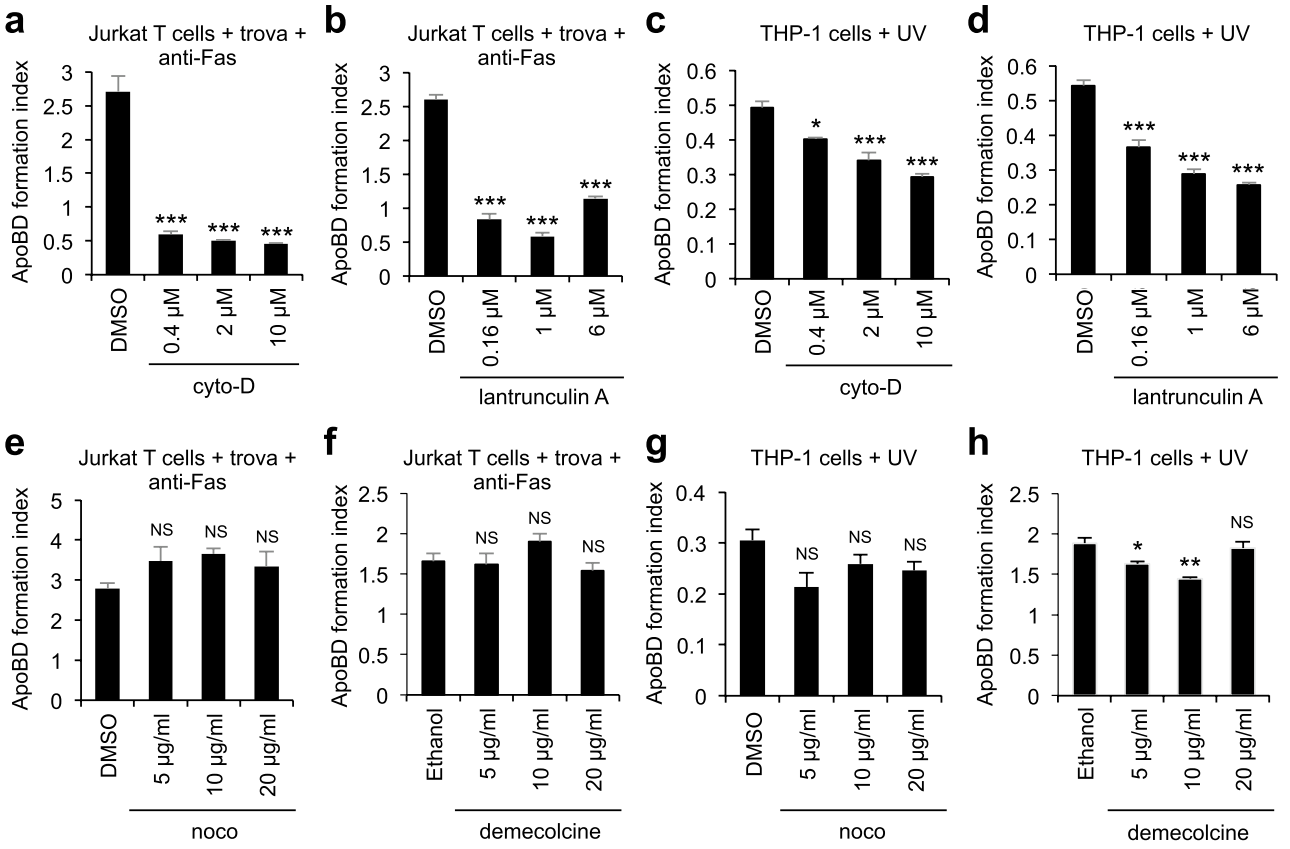

Fig. 4 The effect of pharmacological modulation of F-actin and microtubule assembly on ApoBD formation. The ApoBD formation index (ApoBDs/A5$^+$ apoptotic cells, as measured by flow cytometry) of Jurkat T cells (40 µM trova) in the presence of increasing concentrations of cyto-D (**a**) or lantrunculin A (**b**). ApoBD formation by apoptotic THP-1 monocytes in the presence of increasing concentrations of cyto-D (**c**) or lantrunculin A (**d**). ApoBD formation by apoptotic Jurkat T cells (40 µM trova) in the presence of increasing concentrations of noco (**e**) or demecolcine (**f**). ApoBD formation by apoptotic THP-1 monocytes in the presence of increasing concentrations of noco (**g**) or demecolcine (**h**). Error bars represent SEM (n = 3), data are representative of three independent experiments, NS = $p \geq 0.05$, *$p < 0.05$, **$p < 0.01$, ***$p < 0.001$, one-way ANOVA and Tukey post-hoc test. Apoptosis was induced by 250 ng/mL anti-Fas treatment or 150 mJ/cm^2 UV irradiation for Jurkat T cells or THP-1 cells, respectively.

(Fig. 1g). Next, we stained A431 cells with the cell permeable probes SiR-actin and SiR-tubulin, and monitored the distribution of F-actin and microtubules throughout the course of apoptosis by live confocal microscopy. Approximately 84% and 90% of apoptotic A431 cells generated membrane protrusions rich in F-actin and microtubules, respectively (Fig. 6b–e). Similar to Jurkat T cells, pharmacological inhibition of actin polymerisation had no effect on the ability of A431 cells to form apoptotic membrane protrusions (Fig. 7a, Supplementary Fig. 5) but markedly reduced the formation of ApoBDs (Fig. 7b, c), possibly due to blocking the membrane blebbing stage of apoptotic A431 cell disassembly [33]. In contrast, pharmacological inhibition of microtubule assembly resulted in an impairment of apoptotic membrane protrusion formation (Fig. 7d, Supplementary Fig. 5) but had minimal effect on ApoBD formation by A431 cells (Fig. 7e, f). Collectively, these data suggest that although microtubule assembly is important for the formation of apoptotic membrane protrusions by A431 cells, microtubules do not play a major role in the disassembly of apoptotic A431 cells.

Regulation of apoptotic A431 cell disassembly by PANX1 and vesicular trafficking

The formation of apoptopodia by T cells and monocytes during apoptosis is negatively regulated by caspase-activated PANX1 membrane channels and positively regulated by vesicular trafficking [24, 26]. Thus, we sort to examine whether apoptotic membrane protrusions generated by A431 cells (previously described as microtubule spikes) are also regulated by PANX1 and vesicular trafficking. Addressing these questions could help clarify whether microtubule spikes (as described in Moss et al. [25]) and apoptopodia are distinct forms of protrusions or microtubule spikes are simply a subtype of apoptopodia that are microtubule rich. First, we examined whether PANX1 is activated in A431 cells

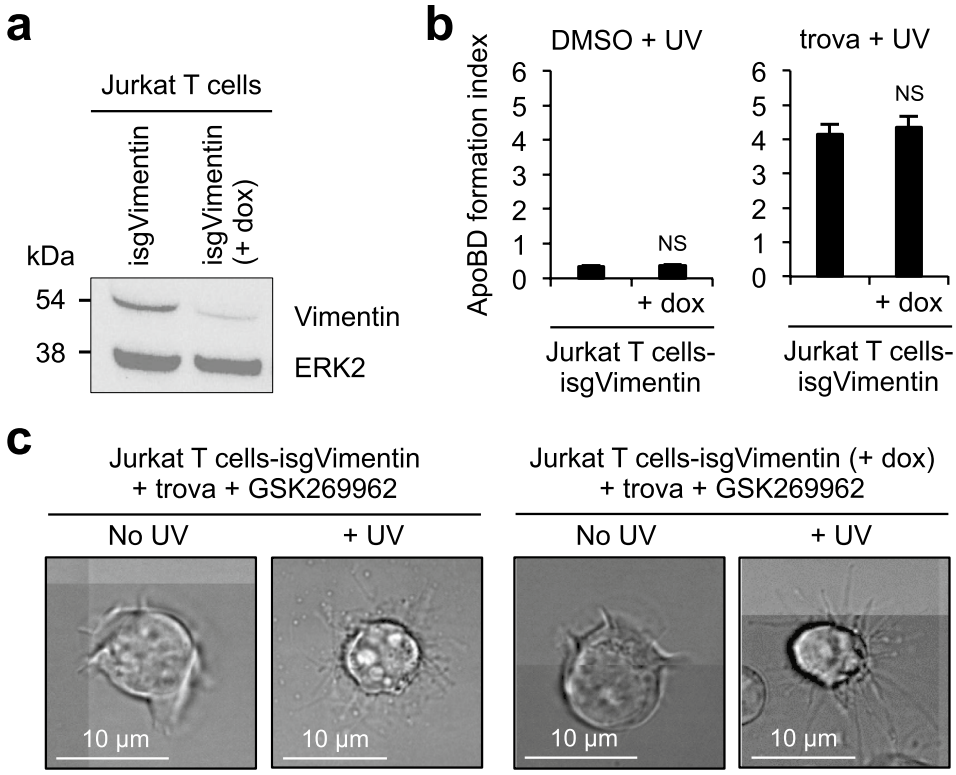

Fig. 5 Knockdown of vimentin has no impact on apoptotic cell disassembly. **a** Reduction in Jurkat T cell vimentin protein expression by CRISPR/Cas9-mediated gene disruption upon dox treatment (1 µg/mL, 3 days). **b** ApoBD formation by untreated and trova (40 µM) treated isgVimentin Jurkat T cell mixed populations with and without dox (1 µg/mL, 3 days). Cas9 only Jurkat T cells used as controls. Error bars represent SEM (n = 3), data are representative of three independent experiments, NS = $p \geq 0.05$, unpaired Student's two-tailed *t* test. **c** Representative confocal microscopy images of viable and apoptotic isgVimentin Jurkat T cell mixed populations (40 µM trova, and 1 µM GSK269962 (ROCK1 inhibitor) to inhibit membrane blebbing to help visualise apoptopodia formation) with and without dox (1 µg/mL, 3 days). Apoptosis was induced by 150 mJ/cm^2 UV irradiation.

during apoptosis and if the disassembly of A431 cells is negatively regulated by PANX1. Immunoblotting demonstrated that similar to Jurkat T cells [38] and THP-1 monocytes [39], A431 epithelial cells express PANX1 and PANX1 is subject to proteolytic cleavage upon apoptosis induction (Supplementary Fig. 6a). It is of interest to note that ROCK1, a positive regulator of apoptotic membrane blebbing following caspase-mediated cleavage, is also expressed by A431 cells and is proteolytically cleaved during apoptosis (Supplementary Fig. 6a). A key function of PANX1 channels is to mediate the passage of small molecules, in particular the release of ATP during apoptosis [38]. Therefore, we utilised a bioluminescence assay to detect ATP in the cell culture supernatant from untreated and UV-treated A431 cells. An increase in ATP in the cell culture supernatant was detected following induction of apoptosis by UV irradiation (Supplementary Fig. 6b). Notably, ATP release by UV-treated A431 cells was also inhibited by the PANX1 inhibitor trova (Supplementary Fig. 6b). To further examine the activation of PANX1 in A431 cells during apoptosis, we measured the uptake of the membrane impermeable nucleic acid binding dye TO-PRO-3 by apoptotic cells, whereby TO-PRO-3 can enter early apoptotic cells via caspase-activated PANX1 channels [38]. Using a flow cytometry-based approach, we observed an increase in TO-PRO-3 uptake by apoptotic A431 cells as compared to viable A431 cells, and the uptake of TO-PRO-3 by apoptotic A431 cells was inhibited by trova (Supplementary Fig. 6c). Next, to examine whether caspase-activated PANX1 is a negative regulator of A431 cell disassembly, PANX1 activity was targeted pharmacologically by trova treatment and apoptotic cell disassembly monitored by time-lapse DIC microscopy and flow cytometry. Although apoptotic A431 cells generated multiple membrane protrusions in the absence of PANX1 inhibition, trova treatment induced a notable increase in A431 cells undergoing cell disassembly (Supplementary Fig. 6d). To better quantify the apoptotic cell disassembly process, ApoBD formation by apoptotic A431 cells was measured by flow cytometry and trova (40 µM) treatment promoted ApoBD formation (Supplementary Fig. 6e). It is worth noting that trova treatment was able to alter the apoptotic cell disassembly process without affecting the levels of apoptosis or necrosis (data

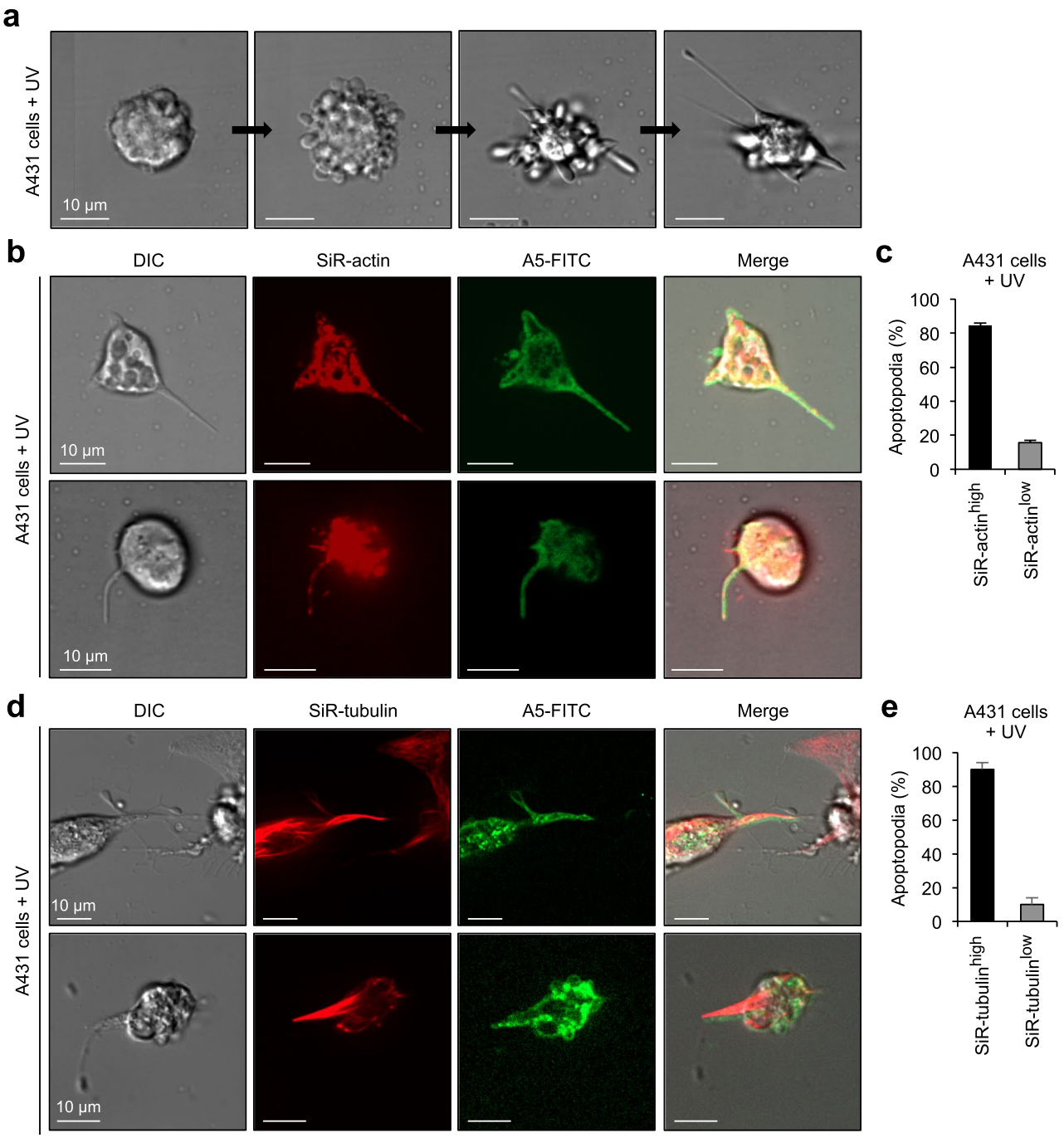

Fig. 6 Localisation of F-actin and microtubules during apoptotic A431 cell disassembly. **a** Representative time-lapse DIC microscopy images of UV-irradiated A431 epithelial cells undergoing apoptotic cell disassembly over 4–5 h. **b** Representative confocal microscopy images of UV-irradiated A431 cells stained with SiR-actin (red) and A5-FITC (green). **c** Quantification of the percentage of apoptotic A431 cells with protrusions containing SiR-actin staining. **d** Representative confocal microscopy images of UV-irradiated A431 cells stained with SiR-tubulin (red) and A5-FITC (green). **e** Quantification of apoptotic A431 cells with protrusions containing SiR-tubulin staining. Error bars represent SEM (n = 3), data are representative of three independent experiments. Apoptosis was induced by 150 mJ/cm^2 UV irradiation.

not shown). In previous studies, the formation of apoptopodia and ApoBDs by apoptotic Jurkat T cells and THP-1 monocytes could be blocked by the antidepressant sertraline [24]. Sertraline was initially identified from a drug screen for inhibitors of ApoBDs, and its mechanism on apoptotic cells was attributed to its possible function in interfering with vesicular trafficking [24]. Similarly, sertraline-treated apoptotic A431 cells also generated less apoptotic membrane

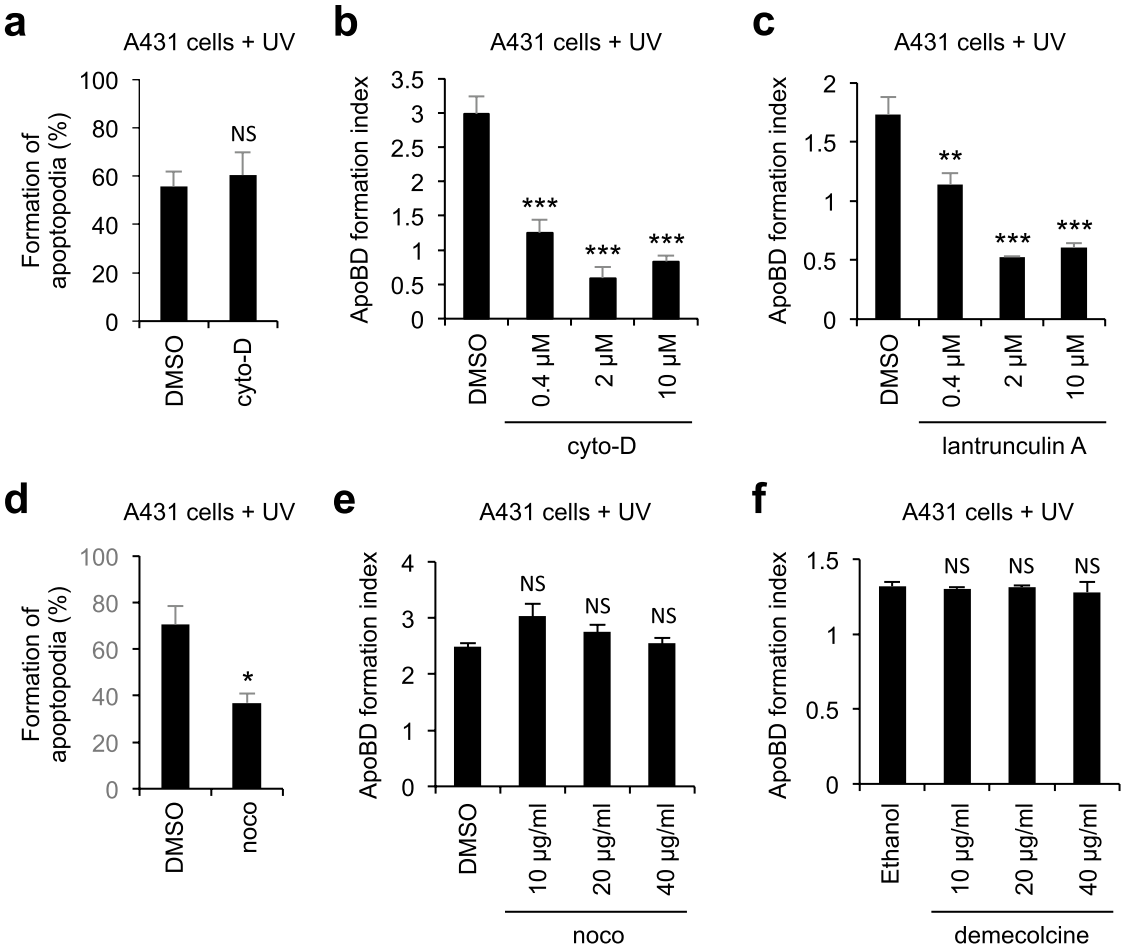

Fig. 7 The role of actin and tubulin polymerisation in apoptotic A431 cell disassembly. **a** Percentage of apoptotic A431 cells forming membrane protrusions, with and without 10 µM cyto-D treatment, at 4–5 h post induction of apoptosis. Generation of ApoBDs by apoptotic A431 cells in the presence of increasing concentrations of cyto-D (**b**) or lantrunculin A (**c**), as measured by flow cytometry. **d** Percentage of apoptotic A431 cells forming membrane protrusions, with and without 20 µg/mL noco treatment, at 4–5 h post induction of apoptosis. ApoBD formation by apoptotic A431 cells in the presence of increasing concentrations of noco (**e**) or demecolcine (**f**), as measured by flow cytometry. Error bars represent SEM (n = 3), data are representative of three independent experiments, NS = $p \geq 0.05$, *$p < 0.05$, **$p < 0.01$, ***$p < 0.001$, one-way ANOVA and Tukey *post-hoc* test (**a**, **d**) or unpaired Student's two-tailed *t* test (**b**, **c**, **e**, **f**). Apoptosis was induced by 150 mJ/cm^2 UV irradiation.

protrusions and ApoBDs as compared to vehicle-treated cells (Supplementary Fig. 6f, g), without affecting the levels of apoptosis or necrosis (data not shown). Together, these data suggest that the mechanism underpinning the disassembly of A431 epithelial cells during apoptosis is similar to other cell types such as T cells and monocytes.

Discussion

Recently, two new types of string-like apoptotic membrane protrusions have been described during the progression of apoptosis, namely apoptopodia and beaded-apoptopodia [24, 26]. Although some mechanistic insights underpinning the generation of these apoptotic membrane protrusions have been described (i.e. regulation by PANX1 and vesicular trafficking), the role of cytoskeletal components in protrusion formation has not been characterised. In comparison to lamellipodia, invadopodia and nanotubes, cell protrusive structures that are reliant on actin polymerisation and remodelling for their formation and function [5, 6, 8, 13], our results indicate that apoptopodia are a distinct subclass of membrane protrusion in which their formation is not dependent on actin polymerisation despite the presence of readily detectable levels of F-actin within apoptopodia. Although actin polymerisation does not appear to provide the protrusive force to promote apoptopodia extension, it does not preclude other roles of F-actin in apoptopodia biology. As described in this study, F-actin was found in most apoptopodia even when actin polymerisation was targeted

pharmacologically, suggesting that F-actin may have other functions within apoptopodia, possibly stabilising the protrusion or parts of it for a period of time. Notably, for well characterised membrane protrusions like filopodia, an influx of water and an increase in hydrostatic pressure can provide the force necessary to push out the membrane and generate filopodia structures [40, 41]. Actin is then thought to polymerise into the already growing filopodia [40], and possibly contribute to protrusion stability [41]. Interestingly, inhibition of actin polymerisation can disrupt filopodia morphology and rigidity [41], similar to the subtle changes in apoptopodia morphology observed in this study after treatment with actin polymerisation inhibitors (Supplementary Figs. 1, 2). Furthermore, the extension rate of growing filopodia is similar to the rate we have described for apoptopodia extension [42]. It is also important to note that the F-actin present in apoptopodia following cyto-D treatment may derive from existing actin filaments in the cell prior to drug treatment, since cyto-D does not destabilise existing F-actin but blocks further actin polymerisation. Nevertheless, how F-actin can localise into apoptopodia and whether actin polymerisation can contribute to apoptopodia stability requires further investigation.

It is well documented that microtubules are an important cytoskeletal component in cells undergoing apoptosis, particularly playing an important role in plasma membrane blebbing and lining the membrane to prevent the early onset of secondary necrosis [23, 43, 44]. Additionally, microtubules were shown to play an important role in the formation of microtubule rich apoptotic membrane protrusions termed microtubule spikes, initially described in human A431 epithelial cells undergoing apoptosis [25]. Consistent with previous studies, the majority (~90%) of apoptotic membrane protrusions generated from A431 cells were found to contain microtubules. In contrast, only a smaller subset of apoptopodia generated from apoptotic Jurkat T cells and THP-1 monocytes (~60% and 20%, respectively) contained microtubules. Interestingly, these observations raise the question whether apoptotic membrane protrusions should be named based on the cytoskeletal components present in the protrusions. Since only a subset of thin apoptotic membrane protrusions generated from apoptotic A431, Jurkat T and THP-1 cells contain microtubules (likewise for F-actin), and most (~90%) of the apoptotic membrane protrusions generated from apoptotic A431 cells also contain F-actin, our findings highlight that apoptotic membrane protrusions should not be named based on their cytoskeletal composition. It is also important to note that noco treatment, which induces microtubule disassembly, only had a minor effect on apoptotic membrane protrusion formation. Furthermore, contrary to the findings of Moss et al. [25], noco treatment had minimal effect on ApoBD formation, suggesting microtubule assembly is not essential for apoptotic cell disassembly. However, these discrepancies between the current and previous studies may be due to differences in the methodologies used to monitor apoptotic cell disassembly as previous studies quantified ApoBD formation following sample fixation and cytospin to collect samples for microscopy analysis [25], whereas ApoBDs were monitored in this study by a flow cytometry-based approach based on the exposure of PtdSer and relative size without extensive sample processing procedures.

One major difference between the membrane protrusions generated from viable cells (such as filopodia and lamellipodia) and apoptopodia by apoptotic cells is their functional roles. Viable cells produce stable membrane protrusions that aid migration and invasion and thus, their function is dependent on the membrane protrusion remaining intact and withstanding surrounding forces. However, apoptopodia remain a unique class of membrane protrusions which are expected to undergo fragmentation to perform their key function (i.e. formation of ApoBDs). In previous studies [26], apoptopodia were found to separate large membrane blebs of apoptotic cells and subsequently generate ApoBDs upon fragmentation of the apoptopodia structure. Thus, it is conceivable that apoptopodia may contain a unique cytoskeletal composition that facilitates protrusion formation before breakage to release ApoBDs.

Finally, the functional roles of thin apoptotic membrane protrusions like apoptopodia are still yet to be fully defined. Nevertheless, the generation ApoBDs via an apoptopodia-dependent mechanism was recently shown to aid the uptake of apoptotic materials by macrophages [33]. Moreover, cell disassembly via the formation of apoptopodia could also alter the distribution of cellular contents into ApoBDs [45]. In addition to the regulation of ApoBD formation, it is possible that thin apoptotic membrane protrusions may directly promote apoptotic vesicle uptake. For example, previously so-called microtubule spikes generated by A431 cells were suggested to facilitate interactions between apoptotic cells and neighbouring phagocytes to promote cell clearance [25]. Since apoptopodia can expose the 'eat-me' signal PtdSer as shown in this study, apoptopodia may also interact with surrounding phagocytes as a possible 'bridging mechanism' to guide the phagocyte to the remaining debris and therefore aid apoptotic vesicle uptake. Moreover, whether these interactions between the apoptotic cell and phagocyte are important to facilitate the cell disassembly process would also be of interest to examine. Furthermore, other cellular protrusions generated by viable cells can have important function in cell motility [2], intercellular communication [46] and environment sensing [47]. For example, immune cell-derived nanotubes can contain important cell surface molecules, such as MHC class I, and these surface molecules can be transferred from cell to cell via connecting nanotubes [46]. With this in mind, it would be of interest to determine the range of surface molecules present on thin apoptotic

membrane protrusions like apoptopodia and whether the generation of apoptopodia could mediate the transfer of cell surface molecules to neighbouring cells. Notably, a number of studies have demonstrated the ability of ApoBDs to aid intercellular communication by transferring cytokines, microRNAs, signalling molecules and cell surface receptors to neighbouring cells [48–51]. Thus, the formation of apoptopodia could potentially facilitate intercellular communication via both direct and indirect (i.e. through ApoBDs) mechanisms.

Taken together our results presented in this study demonstrate that apoptotic membrane protrusions such as apoptopodia represent a unique class of membrane protrusions which can be generated in the absence of certain cytoskeletal components.

Methods

Cell culture

THP-1 monocytes and Jurkat T cells were obtained from ATCC. A431 epithelial cells were obtained from Lonza. ROCK1$^{-/-}$ (clone 1) Jurkat T cells were previously generated by CRISPR/Cas9 technology [33]. Jurkat T cells and THP-1 monocytes were cultured in complete RPMI media (cRPMI) including RPMI 1640 (Life Technologies, 22400-089), 10% (vol/vol) foetal calf serum (FCS) (Gibco, 10099-141) and 50 IU/mL penicillin, 50 µg/mL streptomycin mixture (Life Technologies, 15140122). A431 epithelial cells were cultured in complete MEM (cMEM) including MEM (Lonza), 10% (vol/vol) foetal calf serum (FCS) (Gibco, 10099-141) and 50 IU/mL penicillin, 50 µg/mL streptomycin mixture (Life Technologies, 15140122), L-glutamine and non-essential amino acid (Thermofisher Scientific). All cells lines were cultured at 37 °C, 5% CO_2.

Isolation of primary mouse monocytes and thymocytes

For isolation of primary mouse cells, 6–8 week old C56BL/6 mice (either male or female) were used under approval of AEC15-36, La Trobe University. All experiments were approved by the La Trobe University Animal Ethics Committee in accordance with the National Health and Medical Research Council Australia code of practice for the care and use of animals for scientific purposes. Primary mouse monocytes were isolated from the bone marrow using the negative selection monocyte isolation kit (MACS Miltenyi Biotec), as per the manufactures protocol. To isolate primary thymocytes, the thymus was harvested, homogenised and filtered through a 70 µm cell strainer to generate a single cell suspension.

Induction of apoptosis

To induce apoptosis by UV irradiation, cells were exposed to 150 mJ/cm^2 UV irradiation using the UV Stratagene Stratalinker 1800 (Alient Technologies). Alternatively, to induce Jurkat T cells to undergo apoptosis by anti-Fas treatment for flow cytometry-based assays, cells were incubated with 250 ng/mL anti-Fas [24]. Approximately ~ 80% of Jurkat T cells were apoptotic 4 h post anti-Fas treatment (data not shown). Cells were incubated for 4 h at 37 °C, 5% CO_2 unless otherwise specified.

DIC and fluorescence microscopy

For DIC microscopy including time-lapse imaging, 7.5×10^4 cells were seeded in the wells of a 4 well Nunc® Lab-Tek® II chamber Slide system in either cRPMI or 1% BSA/serum free RPMI medium. A431 cells were imaged in 1% BSA/serum free MEM medium. Additionally, for THP-1 analysis, wells were precoated with 1% poly-l-lysine (Sigma-Aldrich). Apoptosis was induced as above and where specified the following drugs were added: trova (40 µM), cyto-D (10 µM), noco (20 µg/mL) and sertraline (15 µM) immediately after apoptosis induction. Cell samples were imaged for 4 h at 37 °C, 5% CO_2 unless otherwise specified. Imaging was performed using the Zeiss Spinning Disk confocal microscope equipped with a × 63/1.4 oil objective and images were acquired every 2 min.

For imaging of actin and tubulin, cells were incubated overnight in cRPMI containing 1:1000 SiR-actin or SiR-tubulin probes (Spirochrome). Cells were then centrifuged at 300×*g* for 5 min and the plasma membrane was stained with CD45-FITC (1:150, 20 min, ice) or A5-FITC (1:200, 10 min, RT). CD45 was used as a plasma membrane marker for THP-1 cells as the level of PtdSer exposure on apoptotic THP-1 cells during cell disassembly is low (data not shown). Apoptosis was induced as described above and where indicated 10 µM cyto-D or 20 µg/mL noco was added prior to imaging. Time-lapse confocal microscopy was performed by imaging cells every 20 min for 4 h with the Zeiss Spinning Disk confocal microscope, using × 63/1.4 oil objective and incubation was maintained at 37 °C, 5% CO_2. To determine F-actin/microtubule rich (SiR-actin^{high}/SiR-tubulin^{high}) and F-actin/microtubule depleted (SiR-actin^{low}/SiR-tubulin^{low}) apoptotic membrane protrusions, z-stack confocal microscopy images were captured using the same microscopy settings.

Apoptotic protrusion velocity quantification

DIC confocal microscopy analysis was performed as outlined above for THP-1 monocytes or ROCK1$^{-/-}$ Jurkat T cells in 1% BSA/serum free RPMI using the Zeiss Spinning

disk confocal microscope. Apoptosis was induced as above and ROCK1$^{-/-}$ Jurkat T cells were treated with 40 µM trova. For Jurkat T cell and THP-1 monocyte analysis, images were acquired every 2 min and every 5 min for A431 epithelial cells. To determine the average velocity of thin apoptotic membrane protrusion formation, membrane protrusion extension was measured until protrusions began to retract or fragment. Protrusions from approximately 10 cells per experiment were quantified to determine the protrusion formation velocity in µm/min. Scatter plot was constructed by Graph Pad Prism 7.

3D culture imaging

To image apoptotic membrane protrusion formation within a 3D culture, Cultrex® Reduced Growth Factor Basement Membrane Matrix (Trevigen) was used. Briefly, 2.5×10^4 Jurkat T cells, THP-1 monocytes, primary mouse thymocytes and primary mouse monocytes were collected and mixed with 10 µL ice cold Cultrex®. The Cultrex®/cell suspension was then added directly to the centre of a 8 well Nunc® Lab-Tek® II chamber Slide system and incubated at 37 °C for 20 min. Next, 200 µL of 2% Cultrex®/cRPMI was added to each well and cells were incubated for a further 40 min at 37 °C. Apoptosis was induced and imaging performed as outlined above.

Flow cytometry

To quantify ApoBD formation in the presence of cytoskeletal inhibitors, THP-1 monocytes or Jurkat T cells were prepared in 1% BSA/serum free RPMI. A431 cells were prepared in 1% BSA/serum free MEM. Apoptosis was induced as described above and cells were incubated in the respective concentration of trova, cyto-D, lactruculin A, noco, demecolcine or sertraline (drugs were added immediately after induction of apoptosis) for 4 h 37 °C, 5% CO_2. Apoptotic samples were stained with 1:200 A5-FITC and 0.5 µM TO-PRO-3 in 1x A5 binding buffer for 10 min, at RT in the dark. Samples were then kept on ice and in the dark until flow cytometric analysis using the BD FACSCanto II flow cytometer (BD Biosciences). Data analysis was performed as outlined in Jiang et al. [52], using FlowJo software 8.8.10 (Tree Star).

CRISPR/Cas9 gene editing

To generate vimentin deficient Jurkat T cells, a doxycycline-inducible sgRNA vector CRISPR/Cas9 system was used [33, 53]. Briefly, Jurkat T cells stably expressing Cas9 endonuclease were generated as previously described [33]. Vimentin-specific gRNA sequences exon 2 5′-TCCCTCCTACCGCAGGATGTTCGG-3′ and 3′-AAACCCGAACATCCTGCGGTAGGA-5′ were designed using mit.edu.au/CRISPR software [54], annealed and ligated into the Fgh1tUTG plasmid. Jurkat T cells expressing Cas9 were spin infected with lentiviral supernatant containing Fgh1tUTG-vimentin sgRNA and mixed population of sgRNA/Cas9 double positive cells were isolated using FACSAria III cell sorter (BD biosciences). Cells were then treated with 1 µg/mL doxycycline where specified for 3 days to generate gene disruption.

Immunoblotting

Immunoblotting was performed to confirm disruption of vimentin expression by CRISPR/Cas9, and validate PANX1/ROCK1 expression and caspase-mediated cleavage. Approximately 1×10^6 cells were induced to undergo apoptosis where specified (for A431 cells), as described above. Cells were lysed at 4 °C in lysis buffer [20 mM HEPES pH 7.4, 1%, IGEPAL® CA-630, 10% glycerol, 1% Triton X-100, 150 mM NaCl, 50 mM NaF, protease inhibitor cocktail tablet (Roche, CH), phosphatase inhibitor cocktail tablet (Roche)], separated by 10–12% SDS-PAGE gel analysis and immunoblotted with the following antibodies: anti-vimentin (1:1000 clone v9, Santa Cruz), anti-ERK2 (1:1000, clone D-2, Santa Cruz), anti-PANX1 (1:1000, clone D9M1C, Cell Signalling Technologies) and anti-ROCK1 (1:1000, clone H-85, Santa Cruz).

ATP release assay

Approximately 3×10^4 A431 cells were seeded into a 96-well microtitre plate. Cells were untreated or treated with UV irradiation with or without 40 µM trova as specified. After 4 h, cell supernatants were collected following centrifugation at 350×*g* for 5 min and 300×*g* for 5 min and transferred to a 96-well flat-bottom black plate. ATP was detected by a luciferase-based assay, where an equal volume of bioluminescence reagent (Roche Diagnostics) was added to each sample supernatant and endpoint luminescence was recorded on a M5e SpectraMax spectrometer (Molecular Devices). ATP concentration in cultured supernatant was determined from an ATP standard curve.

Statistical analysis

Data are represented as the mean ± the standard error of the mean (SEM). Statistical analysis was performed using a one way ANOVA and *Tukey post-hoc* test or unpaired Students' two-tailed *t*-test. *p*-values less than 0.05 were considered to be significant.

Acknowledgements We thank the La Trobe BioImaging Platform for access to microscopy and flow cytometry equipment and assistance with microscopy. We thank Dr Hendrika Duivenvoorden for

her assistance with 3D cultures. This work was supported by grants from the National Health & Medical Research Council of Australia (GNT1141732, GNT1125033, GNT1140187), Australian Research Council (DP170103790) and La Trobe University (RFA2018).

Author contributions SC, GKAS and IKHP designed and performed experiments with assistance from co-authors. AB generated and performed experiments on vimentin deficient cells. SC, GKAS and IKHP wrote the manuscript with input from co-authors.

Compliance with ethical standards

Competing interests The authors declare no competing financial interests.

References

1. Mattila PK, Lappalainen P (2008) Filopodia: molecular architecture and cellular functions. Nat Rev Mol Cell Biol 9:446–454
2. Small JV et al (2002) The lamellipodium: where motility begins. Trends Cell Biol 12:112–120
3. Davis DM, Sowinski S (2008) Membrane nanotubes: dynamic long-distance connections between animal cells. Nat Rev Mol Cell Biol 9:431–436
4. Eddy RJ et al (2017) Tumor cell invadopodia: invasive protrusions that orchestrate metastasis. Trends Cell Biol 27:595–607
5. Ballestrem C et al (2000) Actin-dependent lamellipodia formation and microtubule-dependent tail retraction control-directed cell migration. Mol Biol Cell 11:2999–3012
6. Schoumacher M et al (2010) Actin, microtubules, and vimentin intermediate filaments cooperate for elongation of invadopodia. J Cell Biol 189:541–556
7. Rustom A et al (2004) Nanotubular highways for intercellular organelle transport. Science 303:1007–1010
8. Pollard TD, Cooper JA (2009) Actin, a central player in cell shape and movement. Science 326:1208–1212
9. Keller KE et al (2017) Tunneling nanotubes are novel cellular structures that communicate signals between trabecular meshwork cells. Invest Ophthalmol Vis Sci 58:5298–5307
10. Pollard TD, Borisy GG (2003) Cellular motility driven by assembly and disassembly of actin filaments. Cell 112:453–465
11. Insall RH, Machesky LM (2009) Actin dynamics at the leading edge: from simple machinery to complex networks. Dev Cell 17:310–322
12. Sheetz MP, Wayne DB, Pearlman AL (1992) Extension of filopodia by motor-dependent actin assembly. Cell Motil Cytoskelet 22:160–169
13. Hanna SJ et al (2017) The role of Rho-GTPases and actin polymerization during macrophage tunneling nanotube biogenesis. Sci Rep 7:8547
14. Isogai T et al (2015) Initiation of lamellipodia and ruffles involves cooperation between mDia1 and the Arp2/3 complex. J Cell Sci 128:3796–3810
15. Vinzenz M et al (2012) Actin branching in the initiation and maintenance of lamellipodia. J Cell Sci 125:2775–2785
16. Svitkina TM, Borisy GG (1999) Arp2/3 complex and actin depolymerizing factor/cofilin in dendritic organization and treadmilling of actin filament array in lamellipodia. J Cell Biol 145:1009–1026
17. Wang YL (1985) Exchange of actin subunits at the leading edge of living fibroblasts: possible role of treadmilling. J Cell Biol 101:597–602
18. Bugyi B, Carlier MF (2010) Control of actin filament treadmilling in cell motility. Annu Rev Biophys 39:449–470
19. Euteneuer U, Schliwa M (1984) Persistent, directional motility of cells and cytoplasmic fragments in the absence of microtubules. Nature 310:58–61
20. Mitchison T, Kirschner M (1988) Cytoskeletal dynamics and nerve growth. Neuron 1:761–772
21. Smith SJ (1988) Neuronal cytomechanics: the actin-based motility of growth cones. Science 242:708–715
22. Martins GG, Kolega J (2012) A role for microtubules in endothelial cell protrusion in three-dimensional matrices. Biol Cell 104:271–286
23. Atkin-Smith GK, Poon IK (2016) Disassembly of the dying: mechanisms and functions. Trends Cell Biol 27:151–162
24. Atkin-Smith GK et al (2015) A novel mechanism of generating extracellular vesicles during apoptosis via a beads-on-a-string membrane structure. Nat Commun 6:7439
25. Moss DK et al (2006) A novel role for microtubules in apoptotic chromatin dynamics and cellular fragmentation. J Cell Sci 119:2362–2374
26. Poon IKH et al (2014) Unexpected link between an antibiotic, pannexin channels and apoptosis. Nature 507:329–334
27. Kerr JF, Wyllie AH, Currie AR (1972) Apoptosis: a basic biological phenomenon with wide-ranging implications in tissue kinetics. Br J Cancer 26:239–257
28. Tixeira R et al (2017) Defining the morphologic features and products of cell disassembly during apoptosis. Apoptosis 22:475–477
29. Mills JC et al (1998) Apoptotic membrane blebbing is regulated by myosin light chain phosphorylation. J Cell Biol 140:627–636
30. Sebbagh M et al (2001) Caspase-3-mediated cleavage of ROCK I induces MLC phosphorylation and apoptotic membrane blebbing. Nat Cell Biol 3:346–352
31. Huot J et al (1998) SAPK2/p38-dependent F-actin reorganization regulates early membrane blebbing during stress-induced apoptosis. J Cell Biol 143:1361–1373
32. Coleman ML et al (2001) Membrane blebbing during apoptosis results from caspase-mediated activation of ROCK I. Nat Cell Biol 3:339–345
33. Tixeira R et al (2019) ROCK1 but not LIMK1 or PAK2 is a key regulator of apoptotic membrane blebbing and cell disassembly. Cell Death Differ. https://doi.org/10.1038/s41418-019-0342-5
34. Kolomeisky AB, Fisher ME (2001) Force-velocity relation for growing microtubules. Biophys J 80:149–154
35. Brangbour C et al (2011) Force-velocity measurements of a few growing actin filaments. PLoS Biol 9:e1000613
36. Battaglia RA et al (2018) Vimentin on the move: new developments in cell migration. F1000Res 7:1796
37. Lanier MH, Kim T, Cooper JA (2015) CARMIL2 is a novel molecular connection between vimentin and actin essential for cell migration and invadopodia formation. Mol Biol Cell 26:4577–4588
38. Chekeni FB et al (2010) Pannexin 1 channels mediate 'find-me' signal release and membrane permeability during apoptosis. Nature 467:863–867
39. Poon IKH et al (2019) Moving beyond size and phosphatidylserine exposure: evidence for a diversity of apoptotic cell-derived extracellular vesicles in vitro. J Extracell Vesicles 8:1608786
40. Loitto VM et al (2007) Filopodia are induced by aquaporin-9 expression. Exp Cell Res 313:1295–1306
41. Karlsson T et al (2013) Fluxes of water through aquaporin 9 weaken membrane-cytoskeleton anchorage and promote formation of membrane protrusions. PLoS One 8:e59901
42. Breitsprecher D et al (2011) Cofilin cooperates with fascin to disassemble filopodial actin filaments. J Cell Sci 124:3305–3318

43. Lane JD, Allan VJ, Woodman PG (2005) Active relocation of chromatin and endoplasmic reticulum into blebs in late apoptotic cells. J Cell Sci 118:4059–4071
44. Sanchez-Alcazar JA et al (2007) The apoptotic microtubule network preserves plasma membrane integrity during the execution phase of apoptosis. Apoptosis. 12: 1195–1208
45. Jiang L et al (2017) Determining the contents and cell origins of apoptotic bodies by flow cytometry. Sci Rep 7:14444
46. Onfelt B et al (2004) Cutting edge: Membrane nanotubes connect immune cells. J Immunol 173:1511–1513
47. Heckman CA, Plummer HK 3rd (2013) Filopodia as sensors. Cell Signal 25:2298–2311
48. Berda-Haddad Y et al (2011) Sterile inflammation of endothelial cell-derived apoptotic bodies is mediated by interleukin-1alpha. Proc Natl Acad Sci USA 108:20684–20689
49. Brock CK et al (2019) Stem cell proliferation is induced by apoptotic bodies from dying cells during epithelial tissue maintenance. Nat Commun 10:1044
50. Ma Q et al (2019) Mature osteoclast-derived apoptotic bodies promote osteogenic differentiation via RANKL-mediated reverse signaling. J Biol Chem 294:11240–11247
51. Zhu Z et al (2017) Macrophage-derived apoptotic bodies promote the proliferation of the recipient cells via shuttling microRNA-221/222. J Leukoc Biol 101:1349–1359
52. Jiang L et al (2016) Monitoring the progression of cell death and the disassembly of dying cells by flow cytometry. Nat Protoc 11:655–663
53. Kueh AJ, Herold MJ (2016) Using CRISPR/Cas9 technology for manipulating cell death regulators. Methods Mol Biol 1419:253–264
54. Hsu PD et al (2013) DNA targeting specificity of RNA-guided Cas9 nucleases. Nat Biotechnol 31:827–832